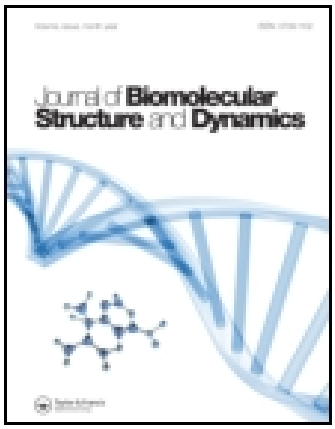

Journal of Biomolecular Structure and Dynamics
Publication details, including instructions for authors and subscription information:
http://www.tandfonline.com/loi/tbsd20

The Effects of Grafting of 2-Pyridyl to $[Ru(bpy)_2(Hpip)]^{2+}$ on Acid-Base and DNA-Binding Properties: Experimental and DFT Studies

An-Guo Zhang [a] , Huai-Xia Yang [a b] & Ke-Zhi Wang [a]
[a] College of Chemistry, Beijing Normal University , Beijing , 100875 , China
[b] Pharmacy College, Henan University of Traditional Chinese Medicine , Zhengzhou , 450008 , China
Published online: 21 May 2012.

To cite this article: An-Guo Zhang , Huai-Xia Yang & Ke-Zhi Wang (2011) The Effects of Grafting of 2-Pyridyl to $[Ru(bpy)_2(Hpip)]^{2+}$ on Acid-Base and DNA-Binding Properties: Experimental and DFT Studies, Journal of Biomolecular Structure and Dynamics, 28:6, 955-968, DOI: 10.1080/07391102.2011.10508621

To link to this article: http://dx.doi.org/10.1080/07391102.2011.10508621

Journal of Biomolecular Structure & Dynamics, ISSN 0739-1102
Volume 28, Issue Number 6, (2011)

The Effects of Grafting of 2-Pyridyl to $[Ru(bpy)_2(Hpip)]^{2+}$ on Acid-Base and DNA-Binding Properties: Experimental and DFT Studies

An-Guo Zhang[1]
Huai-Xia Yang[1,2]
Ke-Zhi Wang[1]*

[1]College of Chemistry, Beijing Normal University, Beijing 100875, China
[2]Pharmacy College, Henan University of Traditional Chinese Medicine, Zhengzhou 450008, China

http://www.jbsdonline.com

Abstract

A new Ru(II) complex of $[Ru(bpy)_2(Hppip)]^{2+}$ {bpy = 2,2′-bipyridine; Hppip = 2-(4-(pyridin-2-yl)phenyl)-1H-imidazo[4,5-*f*][1,10]phenanthroline} has been synthesized by grafting of 2-pyridyl to parent complex $[Ru(bpy)_2(Hpip)]^{2+}$ {Hppip = 2-(4-phenyl)-1H-imidazo[4,5-*f*][1,10]phenanthroline}. The acid-base properties of $[Ru(bpy)_2(Hppip)]^{2+}$ studied by UV-visible and luminescence spectrophotometric pH titrations, revealed off-on-off luminescence switching of $[Ru(bpy)_2(Hppip)]^{2+}$ that was driven by the protonation/deprotonation of the imidazolyl and the pyridyl moieties. The complex was demonstrated to be a DNA intercalator with an intrinsic DNA binding constant of $(5.56 \pm 0.2) \times 10^5\ M^{-1}$ in buffered 50 mM NaCl, as evidenced by UV-visible and luminescence titrations, reverse salt effect, DNA competitive binding with ethidium bromide, steady-state emission quenching by $[Fe(CN)_6]^{4-}$, DNA melting experiments and viscosity measurements. The density functional theory method was also used to calculate geometric/electronic structures of the complex in an effort to understand the DNA binding properties. All the studies indicated that the introduction of 2-pyridyl onto Hpip ligand is more favorable for extension of conjugate plane of the main ligand than that of phenyl, and for greatly enhanced ct-DNA binding affinity accordingly.

Key words: Ruthenium; DNA; Bipyridine; Phenanthroline; Density functional theory.

Introduction

The intriguing photophysical, photochemical, and electrochemical properties (1-3) of Ru(II) polypyridyl complexes have attracted extensive attention in the past decades with regard to their applications in several research areas, including bio-inorganic and biomedicinal chemistry (4, 5), such as DNA cleavage reagents (6-8), DNA molecular light switches (9-11), inhibiting of DNA transcription (12), DNA-dependent electron transfer probes, chemical and stereoselective probes of nucleic acid structures, as well as antitumor drugs (13-15). Ru(II) polypyridyl complexes can interact with DNA noncovalently through electrostatic, groove, and intercalative (including classic intercalation, semi-intercalction and quasi-intercalation) binding modes (16). Many studies have revealed that the planarity of the main ligand plays a key role in the binding mode and affinity (16-19). The ancillary ligand can also indirectly affect the DNA binding properties through changing the planarity of the main ligand and the hydrophobicity of the complex (20). Variations of substituents or substitution position in the main ligand, even a subtle change of molecular structure, may result in some interesting differences in the space configuration and the electron density distribution of Ru(II) polypyridyl complexes, and accordingly the spectral properties and the DNA-binding behaviors of the complexes, providing a chance to explore valuable conformation- or site- specific DNA probes (21, 22).

*Phone: +86-10-58805476
Fax: +86-10-58802075
E-mail: kzwang@bnu.edu.cn

The Ru(II) polypyridyl system with planarity and ancillary ligand presents similarity and contrasts to many of the systems such as the actinomycins, porphyrins, Hoechst and benzo[a]pyrene derivatives and others in forming complexes with the nucleic acids (23-30).

Among Ru(II) complexes reported for DNA-biding studies, 2-phenylimidazo [4,5-*f*] [1,10]-phenanthroline (Hpip)-based complexes have invoked considerable interest (12, 31-42). Ji and co-workers performed systematic studies on the effects of the electronic and geometric (the shape, size, planarity and the intramolecular hydrogen bond) structures of the intercalative ligands on the DNA-binding affinity (31, 32) and DNA cleavage ability (32-34) of the complexes. Our group have reported imidazole-containing Ru(II) complexes with interesting pH-induced emission switch, and/or DNA binding and DNA molecular light switching properties (35-42).

Studies on $[Ru(bpy)_2(Hbpip)]^{2+}$ {Hbpip = 2-(4-biphenyl)imidazo[4,5-*f*][1,10] phenanthroline} carried out by Ji and co-workers (32) showed that it can intercalate into DNA base pairs with a binding constant of $1.7 \times 10^5\ M^{-1}$, which is much lower than that ($4.7 \times 10^5\ M^{-1}$) of the parent complex $[Ru(bpy)_2(Hpip)]^{2+}$ (43). It indicated that a grafting of benzene ring to Hpip ligand of the parent complex $[Ru(bpy)_2(Hpip)]^{2+}$ leads to an unfavorable effect on the DNA-binding affinity of the complex. This can be mainly attributed to the poor planarity of the intercalative ligand Hbpip of $[Ru(bpy)_2(Hbpip)]^{2+}$. However, in this work, we have reported a Ru(II) complex of $[Ru(bpy)_2(Hppip)]^{2+}$ {Hppip = 2-(4-(pyridin-2-yl) phenyl)imidazo[4,5-*f*][1,10]phenanthroline} with introduction of a 2-pyridyl ring onto Hpip ligand of the parent complex $[Ru(bpy)_2(Hpip)]^{2+}$. The studies demonstrated that the introduction of the pyridine ring onto Hpip ligand enhances the DNA-binding affinity ($K_b = 5.56 \times 10^5\ M^{-1}$) of $[Ru(bpy)_2(Hppip)]^{2+}$ moderately compared to analogous complexes of $[Ru(bpy)_2(Hpip)]^{2+}$ and $[Ru(bpy)_2(Hbpip)]^{2+}$ (32, 43). Also, appending of 2-pyridyl to Hpip enriches the acid-base properties of $[Ru(bpy)_2(Hppip)]^{2+}$ with pH-induced off-on-off emission switches.

Recently, theoretical studies have shown that density functional theory (DFT) can predict some properties of Ru(II) complexes successfully (31, 43), because DFT calculations can better consider electron correlation energies, obviously reducing the computational expenses and suit such a kind of complexes with single state (44, 45). These theoretical efforts are very significant in guiding the effects of geometric/electronic structures on the DNA-interacting properties as well as the functional molecular design of this kind of Ru(II) complex (46, 47). In this work, DFT-B3LYP method was also used to calculate geometric/electronic structures of the complex for revealing the factors affecting DNA-binding affinities of analogous complexes of $[Ru(bpy)_2(Hppip)]^{2+}$.

Materials and Methods

Materials

Cis-$[Ru(bpy)_2Cl_2]\cdot 2H_2O$ (40) and 1,10-phenanthroline-5,6-dione (49) were synthesized according to the literature methods. Solvents were purified and dried according to the standard methods (50). The other materials were obtained from commercial sources and were used without further purification. The synthetic route to $[Ru(bpy)_2(Hppip)]^{2+}$ is shown in Scheme 1 (A), and the synthetic details are given below.

Synthesis

2-(4-(Pyridin-2-yl)phenyl)imidazo[4,5-*f*][1,10]phenanthroline (Hppip): A mixture of 4-(pyridin-2-yl)benzaldehyde (0.274 g, 1.5 mmol), 1,10-phenanthroline-5,6-dione (0.315 g, 1.5 mmol) and ammonium acetate (2.47 g, 32 mmol) dissolved in

glacial acetic acid (20 mL), was refluxed for 6 h under N_2 and was then cooled to room temperature. The cooled solution was filtered, diluted with water (90 mL) and neutralized with concentrated aqueous ammonia. A straw yellow precipitate was filtered and washed with a small amount of water, diethyl ether, and then recrystallized from EtOH. Yied: 0.326 g (58.2%). ^{1}H NMR (400 MHz, Me_2SO-d_6) δ/ppm: 9.06 (dd, $J_1 = 4.1$, $J_2 = 1.7$, 2H); 8.96 (dd, $J_1 = 7.9$, $J_2 = 1.7$, 2H); 8.74 (m, 1H); 8.40 (q, $J_1 = 6$, $J_1 = 8.6$, 4H); 8.12 (d, $J = 7.9$, 1H), 7.95 (td, $J_1 = 7.9$, $J_2 = 2.07$, 1H); 7.86 (br, 2H); 7.42 (m, 1H). Anal. Calcd for $C_{24}H_{15}N_5 \cdot 0.5H_2O$ (F.W = 382.42) : C, 75.38; N, 18.31; H, 4.22%. Found: C, 75.54; N, 18.31; H, 4.86%.

$[Ru(bpy)_2(Hppip)](ClO_4)_2 \cdot 2H_2O$: A solution of cis-$[Ru(bpy)_2Cl_2] \cdot 2H_2O$ (0.260 g, 0.5 mmol) and Hppip (0.187 g, 0.5 mmol) in EtOH/H_2O (v/v = 2:1, 120 mL) was heated at 80°C under N_2 for 8 h. The solvent was removed by rotary evaporation, and resulting crude product was purified by column chromatography on silica gel

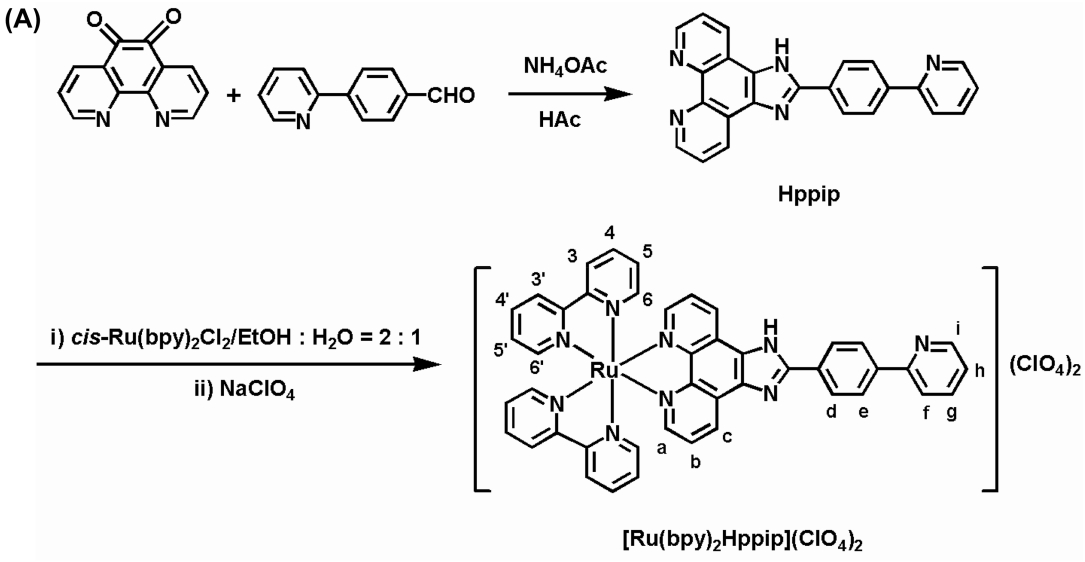

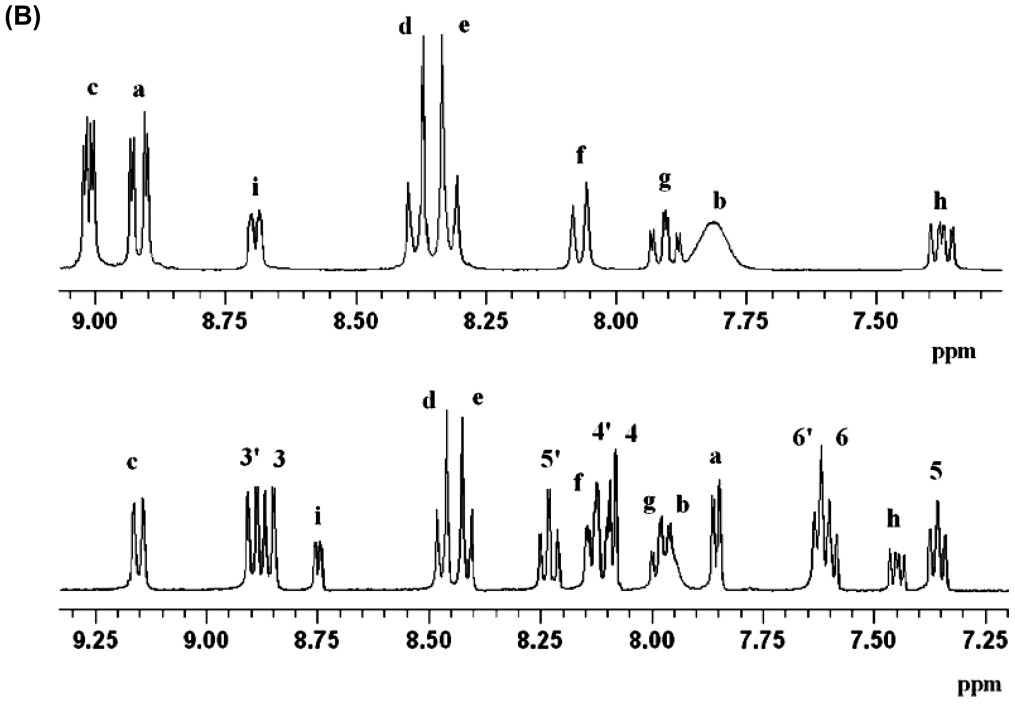

Scheme 1: Synthetic routes to Hppip ligand and $[Ru(bpy)_2(Hppip)](ClO_4)_2$ (**A**). ^{1}H NMR spectra of Hppip (top) and $[Ru(bpy)_2(Hppip)](ClO_4)_2$ (bottom) in Me_2SO-d_6 (**B**).

with saturated aqueous KNO_3-H_2O-MeCN (1:4:40, v/v/v). After addition of saturated $NaClO_4$ aqueous solution and recrystallization from MeCN-diethyl ether, a red product was obtained in a yield of 75.2% (0.322 g). Caution: Perchlorate salts of metal complexes with organic ligands are potentially explosive. Although no detonation tendencies have been observed, caution is advised and handling of only small quantities is recommended. ^{1}H NMR (400 MHz, Me_2SO-d6) δ/ppm: 9.15 (d, J = 7.6, 2H); 8.88 (dd, J_1 = 15.2, J_2 = 8.2, 4H); 8.75 (d, J = 3.9, 1H); 8.44 (q, J_1 = 22.6, J_2 = 8.7, 4H); 8.23 (td, J_1 = 8.1, J_2 = 1.4, 2H); 8.10 (m, 5H); 7.98 (m, 3H); 7.86 (d, J = 5.0, 2H); 7.06 (m, 4H); 7.45 (dd, J_1 = 7.5, J_2 = 4.8, 1H); 7.36 (t, J = 6.7, 2H). Anal. Calcd for $C_{44}H_{31}Cl_2N_9O_8Ru{\cdot}2H_2O$ (F.W = 1021.78): C, 51.75; N, 12.33; H, 3.45%. Found: C, 51.80; N, 12.42; H, 3.32%. Anal. Calcd for MALDI-TOF MS m/z: 886.12 ($[M - ClO_4^-]^+$), 393.43 ($[M - 2ClO_4^-]^{2+}$). Found: 886.15 ($[M - ClO_4^-]^+$), 393.56 ($[M - 2ClO_4^-]^{2+}$).

The identity of the complex was characterized by ^{1}H NMR, IR spectroscopy, luminescence, UV-vis spectroscopy, elemental analysis and MALDI-TOF mass spectrometry. The ^{1}H NMR spectra of $[Ru(bpy)_2(Hppip)](ClO_4)_2$ and Hppip are compared in Scheme 1 (B). The proton resonance signals for the ligand and the complex were assigned by comparisons with those of similar compounds $[Ru(bpy)_2(Hbpip)]^{2+}$ and $[Ru(bpy)_2(Happip)]^{2+}$ (32, 37).

Physical Measurements

Elemental analyses (C, N, and H) were performed on a Vario EL elemental analyzer. ^{1}H NMR spectra were collected on a Bruker DRX-400(300) NMR spectrometer with Me_2SO-d_6 as solvent at room temperature. Matrix-assisted laser desorption ionization mass spectra (MALDI-TOF MS) were run on API Q-star pulsar (Applied Biosystems) mass spectrometer. Infrared spectra were recorded on a Nicolet Avtar 360FT-IR spectrometer as KBr disks. UV-visible spectra were obtained on a GBC Cintra 10e UV-visible spectrometer. Emission spectra were obtained on a Shimadzu RF-5301PC spectrofluorimeter.

UV-visible and emission spectrophotometric pH titrations of the complex were carried out in buffer A: 40 mM H_3BO_3, 40 mM H_3PO_4, 40 mM CH_3COOH, with additions of concentrated sulfuric acid, saturated sodium hydroxide aqueous solution, respectively, to cover the pH range studied. All the experiments involving the interaction of the complex with ct-DNA were carried out in aerated buffer B: 5 mM Tris-HCl, 50mM NaCl, pH = 7.10 ± 0.02. The luminescence quantum yields were calculated by comparison with $[Ru(bpy)_3]^{2+}$ (φ = 0.033) (51) in aerated aqueous solution at room temperature using eq 1, where φ and φ_{std} are the quantum yields, A and A_{std} are the absorbances at the excitation wavelength, and I and I_{std} are the integrated emission intensities for the unkown and standard samples, respectively.

$$\varphi = \varphi_{std}(A_{std}/A)(I/I_{std}) \quad [1]$$

A solution of DNA gave a ratio of UV absorbance at 260 and 280 nm of ca. 1.9:1, indicating that the DNA was sufficiently free of protein. The concentration of DNA in bp was determined spectrophotometrically by assuming ε_{260} = 13200 M^{-1} cm^{-1} (52). The absorption titration with ct-DNA was carried out by keeping the concentration of the Ru(II) complex constant while varying the DNA concentrations. The competitive binding of ethidium bromide (EB) to the DNA with the Ru(II) complex was carried out by measuring EB emission (λ_{ex} = 537 nm) while keeping [DNA]/[EB] = 5 constant but varying Ru(II) complex concentrations. Emission titrations were carried out in buffer B but with varied concentrations of salts. Thermal denaturations of the DNA were performed on a UV-vis spectrophotometer in buffer C: 1.5 mM Na_2HPO_4, 0.5 mM NaH_2PO_4, 0.25 mM Na_2EDTA. With the use of the thermal melting program, the temperature of the cell containing the cuvette was ramped from 50 to 90°C, and the absorbances at 260 nm were measured every 0.5°C.

Viscosity experiments used an Ubbelohde viscometer, immersed in a thermostated water-bath maintained at 32.20 ± 0.02°C. The DNA samples, approximately 200 base pairs in average length, were prepared by sonication in order to minimize complexities arising from DNA flexibility (53). Data were presented as $(\eta/\eta_0)^{1/3}$ versus the ratio of the concentration of Ru(II) complex to that of DNA, where η and η_0 are the viscosities of DNA solutions in the presence and the absence of complex, respectively. Viscosity values were calculated from the observed flowing time of DNA containing solutions (t) corrected for that of buffer alone (t_0), $\eta = t - t_0$ (54).

Computational Methods

Structural schematic diagrams of $[Ru(bpy)_2(Hppip)]^{2+}$ are shown in Scheme 2. The complex forms from a Ru(II) ion, one main ligand Hppip and two ancillary ligands (bpy). The complex has not any symmetry, whereas their parent complex $[Ru(bpy)_3]^{2+}$ for comparison belongs to D3 symmetry. Geometry optimization computations were performed applying the DFT-B3LYP method (55) and LanL2DZ basis set (ECP+DZ for the Ru atom and D95 for C, N, O, H atoms) (56), and assuming the singlet state for the ground state of the complex (57). All the computations were performed with the G03 quantum chemistry program-package (58).

Results and Discussion

Computed Geometrical Structures of the Complex

Computed data of the selected bond lengths and dihedral angles for $[Ru(bpy)_2(Hppip)]^{2+}$ **1** were listed in Table I along with those for the parent complex $[Ru(bpy)_2(Hpip)]^{2+}$ **2** (43) and the analogous complex $[Ru(bpy)_2(Hbpip)]^{2+}$ **3** (32) for comparison. The computed geometric structures using DFT-B3LYP and LanL2DZ level are rather reliable as comparison with crystal structure of $[Ru(bpy)_3]^{2+}$ and computed results for **2** and **3** previously reported (32, 43).

Some structural characteristics can be seen from Table I: (1) Ru-N mean bond length (0.2107 nm) of the main ligand for $[Ru(bpy)_2(Hppip)]^{2+}$ is slightly longer than that (0.2097 nm) of the co-ligand; (2) the mean bond length (0.1400–0.1407 nm) of ligand skeleton for the complex is very close to its standard bond length (0.1400 nm) (60), and that of the main ligand skeleton is also slightly larger than that of the co-ligand; (3) the calculated geometric data of the complex indicate that the grafted pyridine ring is almost co-planer with Hpip framework (dihedral angles are N_5-C_6-C_7-C_8 = -0.29° and C_9-C_{10}-C_{11}-N_{12} = -0.03°) compared with those of the parent complex $[Ru(bpy)_2(Hpip)]^{2+}$ (N_5-C_6-C_7-C_8 = 0.93°) and the analogous complex $[Ru(bpy)_2(Hbpip)]^{2+}$ (N_5-C_6-C_7-C_8 = -0.13° and C_9-C_{10}-C_{11}-C_{12} = -31.45°). Energies of the frontier molecular orbitals for **1** and **3** obtained based on the optimized geometrical structures are shown in Scheme 3 along with those of complex **2** (43) for comparison. And the population and energy levels of the main frontier molecular orbitals for **1** and **3** are compared in Figure S1 (supporting information).

pH Effects on UV-visible and Emission Spectra

pH dependence of the ground state and excited state properties of $[Ru(bpy)_2(Hppip)]^{2+}$ was investigated in buffer A over the pH range of 0.17-12.86. All spectral changes with pH were reversible. As shown in in Figure 1, changes of the UV-vis spectra of the complex as a function of pH, the complex underwent three successive deprotonation

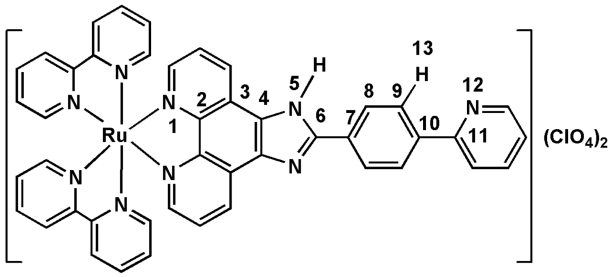

$[Ru(bpy)_2(Hppip)](ClO_4)_2$ **1**

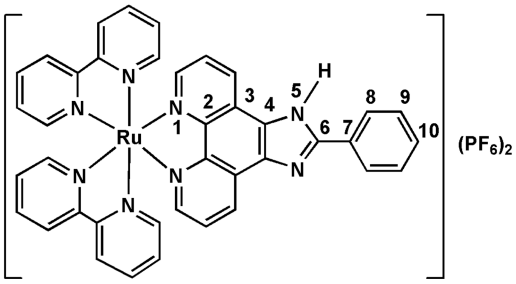

$[Ru(bpy)_2(Hpip)](PF_6)_2$ **2**

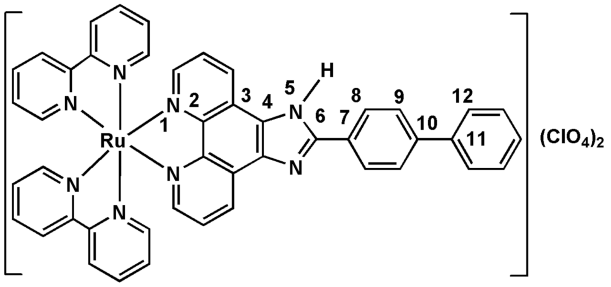

$[Ru(bpy)_2(Hbpip)](ClO_4)_2$ **3**

Scheme 2: Structural schematic diagrams and atomic labels of $[Ru(bpy)_2(Hppip)](ClO_4)_2$ **1**, $[Ru(bpy)_2(Hpip)](PF_6)_2$ **2** [43], and $[Ru(bpy)_2(Hbpip)](ClO_4)_2$ **3**.

processes upon increasing pH from 0.17 to 12.86. Upon increasing pH from 0.17 to 2.76, the absorbance of the bands at 280 and 458 nm increased visibly with a bathochromic shift of 3 nm, the absorption intensities at 318 nm were decreased sharply, and wave valley at 380 nm increased in the intensities with appearance of one isosbestic point at 338 nm. The spectral changes observed above are due to

Table I
Computational selected bond lengths (nm), bond angles (°), and dihedral angels (°) using the DFT-B3LYP at the LanL2DZ level.

									Dihedral angles[d]		
Com. (calc.)	Ru-N_m[a]	Ru-N_{co}	C-C(N)$_m$[b]	C-C(N)$_{co}$	A_m[c]	A_{co}	C_6-C_7	C_{10}-C(N)$_{11}$	N_5-C_6-C_7-C_8	C_9-C_{10}-C(N)$_{11}$-C(N)$_{12}$	ref
1	0.2107	0.2097	0.1407	0.1400	79.31	78.47	0.1458	0.1491	-0.29	-0.03	This work
2	0.2108	0.2097	0.1406	0.1400	79.26	78.47	0.1463	—	0.93	—	43
3	0.2108	0.2097	0.1407	0.1400	79.29	78.48	0.1457	0.1486	-0.13	-31.45	This work

[a]Ru-N_m expresses the mean coordination bond length between Ru and N atoms of the main ligand L, and Ru-N_{co} expresses that between Ru and N atoms of the co-ligand (phen). [b]C-C_m expresses the mean bond length of the ring skeleton of the main ligand, and C-C_{co} expresses that of the co-ligand. [c]A_m expresses the mean coordination bond angle between central Ru and two N atoms of the main ligand, and A_{co} expresses that of the co-ligand. [d]The dihedral angles of complexes **1**, **2**, **3** were computed by us.

one proton dissociation of the protonated imidazole ring of Hpip moiety. Further increasing pH from 2.55 to 5.35 induced the second deprotonation step which is assigned to the proton dissociation of the protonated pyridyl moiety, resulting in the intensity increases in band at 283 nm with a bathochromic shift of 3 nm, the wave valley at 310 nm increased sharply while the dexter wave shoulder of ppip π-π^*-transition band became reduced with an isosbestic point appearing at about 333 nm. The third deprotonation, which was assigned to the deprotonation of the proton on the neutral imidazole ring, took place over pH 7.27-10.86, accompanying the following spectral features: the absorption at 286 nm decreased and the MLCT broad band centered at 460 nm increased with a red shift of 2 nm. The three successive protonation/deprotonation processes occurred for **1** are summarized in Scheme 4. The negative logarithms of three ground-state ionization constant values, pK_{a1} = 1.77 ± 0.01, pK_{a2} = 3.70 ± 0.04, pK_{a3} = 9.03 ± 0.04 were derived for $[Ru(bpy)_2(Hppip)]^{2+}$ by nonlinear sigmoidal fit of the data in the insets of Figure 1. The pK_{a1}, pK_{a2} and pK_{a3} values fall within reasonably pH ranges as comparisons with the pK_{a1} and pK_{a2} values (pK_{a1} = 0.31-2.48 and pK_{a2} = 8.21-9.65) we previously reported for the imidazole ring-containing Ru(II) complexes (35-39), and pK_a = 3.2-3.6 for uncoordinated pyridyl group on $[Ru(bpy)_2(qp)]^{2+}$ (qp = 4,4':2',2'':4'',4'''-quaterpyridine) and $[Ru(bpy)_2(tpy)]^{2+}$ (tpy = 2,2':4',4''-terpyridine) reported by Ward (59).

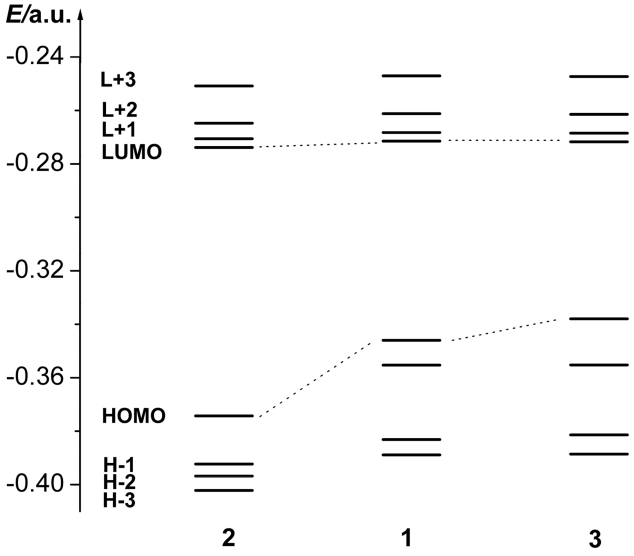

Scheme 3: Schematic map of energies of some frontier molecular orbitals of $[Ru(bpy)_2L]^{2+}$ (L = Hpip 2 [43]; Hppip **1**; Hbpip **3**.

Changes in luminescence spectra of the complex in water as a function of pH are shown in Figure 2, which shows that the emission spectra are sensitive to pH, and consisting of two separate excited-state proptonation/deprotonation processes. Upon increasing pH from 0.17 to 4.56, the emission intensities increased sharply by a factor of ~2.5, and the emission maxima are blue-shifted from 629 to 607 nm, which is different from the intensity enhancement by only 11.6% exhibited by $[Ru(bpy)_2(Hpip)]^{2+}$. Obviously, the spectral changes above are mainly contributed to the excited-state deprotonation of the pyridyl moiety on $[Ru(bpy)_2(Hppip)]^{2+}$. The emission was quenched at the lower pH because the protonated pyridyl moiety could act as an electron acceptor, similarly to the behaviors of pyridyl-containing Ru(II) complexes previously reported (61). In contrast, the further increases in pH from 5.35 to 10.27 reduced the emission intensities by 39%, and elicited a big red-shift of the emission maxima from 607 to 618 nm. This behavior may involve rapid

radiationless decay (57). It has been known that the energy of the metal-centered excited states depends on the ligand field strength, which in turn depends on the σ-donor and π-acceptor properties of the ligands (57). The negative charge on the deprotonated imidazol substituent may be delocalized over the whole π framework, which decreases the σ-donor and increases the π-acceptor capacity of the ppip

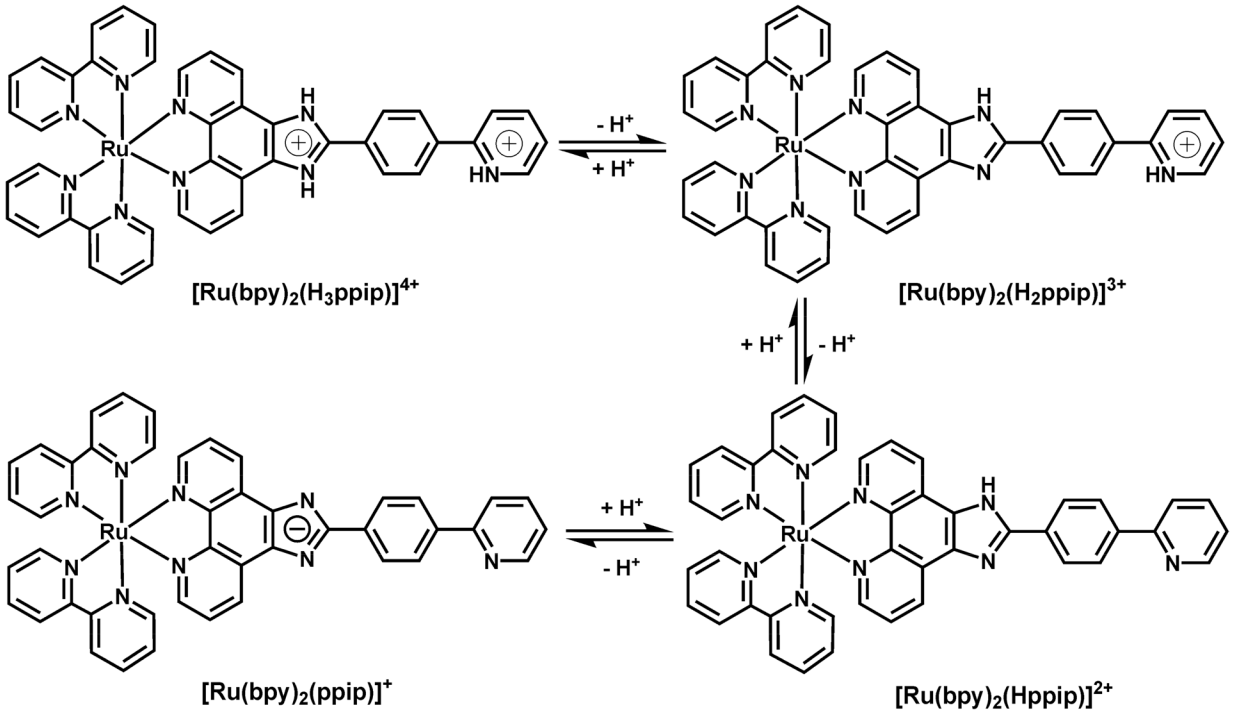

Scheme 4: Protonation/deprotonation processes of $[Ru(bpy)_2(Hppip)]^{2+}$.

ligand, resulting in weakening of the ligand-field strength around the metal center and in turn lowering the metal σ* orbitals (62-64). The grafting of 2-pyridyl group on $[Ru(bpy)_2(Hpip)]^{2+}$ have made the complex $[Ru(bpy)_2(Hppip)]^{2+}$ to exhibit pH induced off-on-off emission switches, although the emission intensity on-off ratio need to be improved.

The ground- and excited-state ionization constants are related thermodynamically by a Förster cycle (61). The Förster treatment results in eq 2, which describes the relationship between the ground-state pK_a and excited-state pK_a* based on pure 0-0 transitions in wave numbers of ν_B and ν_{HB} for the basic and acidic species, respectively (65).

$$pK_a^* = pK_a + (0.625/T)(\nu_B - \nu_{HB}) \qquad [2]$$

In reality, the ν_B and ν_{HB} values are often difficult or even impossible to obtain. A good approximation is to use the emission maxima for ν_B and ν_{HB} since protonation equilibrium is almost certainly established between the ^{3}MLCT states. Therefore, the energies of the emission maxima in wavenumbers were used in eq 2, and two excited-state ionization constants of $pK_{a1}^* = 2.98$ and $pK_{a3}^* = 8.41$ were thus obtained. The value of pK_{a3}^* is comparable to the corresponding pK_{a3} while the value of pK_{a1}^* is 1.21 pK_a units greater than pK_{a1}, indicating that the electron density was significantly higher in the exited state than in the ground state for $[Ru(bpy)_2(H_3ppip)]^{4+}$ and the excited electron was localized on $[H_3ppip]^{2+}$ rather than bpy ligands, while the electron density in the excited state of $[Ru(bpy)_2(Hppip)]^{2+}$ was localized on bpy rather than Hppip.

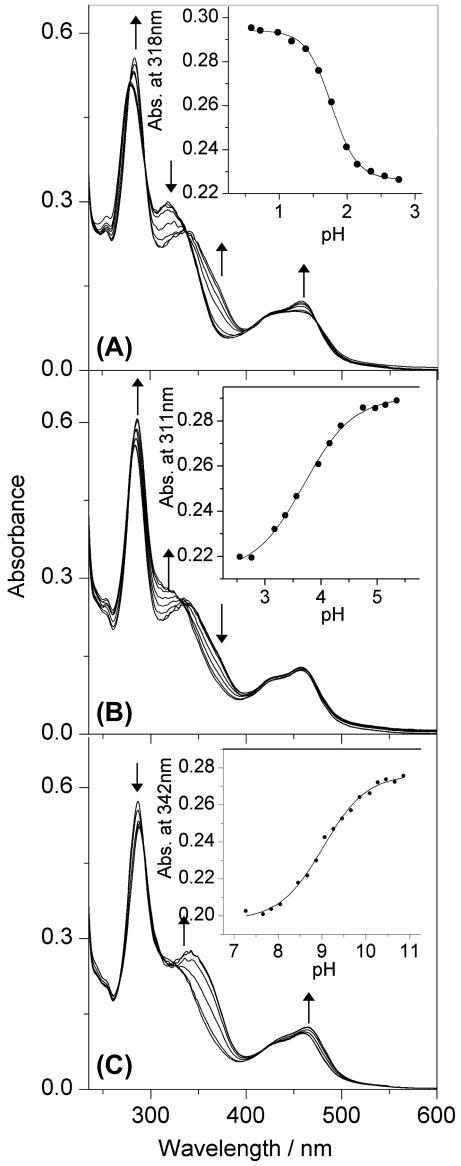

Figure 1: pH effects on the UV-vis spectra of $[Ru(bpy)_2(Hppip)]^{2+}$ (5.0 μM). (**A**) pH = 0.17-2.76; (**B**) pH = 2.55-5.35; (C) pH = 7.27-10.86. Arrows show spectral changes upon increasing pH.

UV-Vis Absorption Spectra: UV-visible and luminescence spectroscopy are two of the most useful techniques for DNA-binding studies of metal complexes. The UV-vis absorption spectra of the complex in neutral aqueous solution mainly consist of two well-resolved bands: one centered at ~286 nm are assigned to an intraligand π-π^*-transitions of bpy ligand, and the other one at ~460 nm are attributed to the metal-to-ligand charge-transfer (MLCT) transition in comparisons with a π-π^* absorption band at 283, 284 and 285 nm and a MLCT band at 458, 458 and 459 nm reported for analogous complexes of $[Ru(bpy)_2(Hpip)]^{2+}$, $[Ru(bpy)_2(Hcip)]^{2+}$ {Hcip = 2-(4-chloro-phenyl)imidazo[4,5-*f*][1,10]phenanthroline}, and $[Ru(bpy)_2(HOP)]^{2+}$ {HOP = 2-(4-hydroxyphenyl)imidazo[4,5-*f*][1,10]phenanthroline}, respectively (66–68). It can be concluded that there are no obvious substituent effects on the bpy intraligand π-π^* and MLCT transitions of the $[Ru(bpy)_2(Hpip)]^{2+}$ system.

The UV-vis absorption spectra of the complex in the absence and the presence of ct-DNA are illustrated in Figure 3A. Upon increasing concentrations of the DNA from 0 to 13 μM (bp), the absorption bands at 286 nm, 320 nm and 460 nm displayed clear hypochromicities with high hypochromism $H\%$ {$H\% = (A_{free} - A_{bound})/A_{free}$} values of 32%, 35% and 26%, respectively. The presence of an isosbestic point at 472 nm indicated the coexistence of free and DNA-bound Ru(II) complex in the solution. The intrinsic DNA binding constant K_b illustrating the binding strength of the complex with ct-DNA was determined from the decay of the absorbance at 286 nm by employing eq 3 (69):

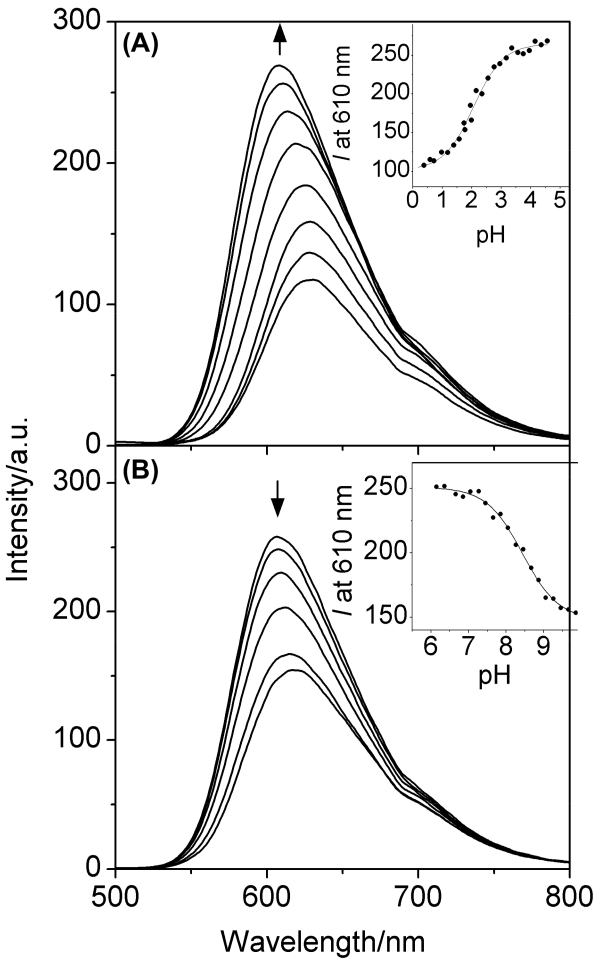

Figure 2: pH effects on the emission spectra (λ_{ex} = 462 nm) of $[Ru(bpy)_2(Hppip)]^{2+}$ (5.0 μM) as a function of pH. (**A**) pH = 0.17-4.56; (**B**) pH = 5.35-10.27. Arrows show spectral changes upon increasing pH.

$$[DNA]/(\varepsilon_a - \varepsilon_f) = [DNA]/(\varepsilon_b - \varepsilon_f) + 1/\{K_b(\varepsilon_b - \varepsilon_f)\} \quad [3]$$

where [DNA] is the DNA concentration in base pairs, ε_a is the apparent absorption coefficient calculated as A_{abs}/[Ru], ε_b and ε_f are the extinction coefficients for the free and bound forms of the ruthenium complex. In a plot of $[DNA]/(\varepsilon_a - \varepsilon_f)$ versus [DNA], K_b is given by the ratio of the slope to the *y* intercept. An intrinsic DNA binding constants K_b for 1 was derived to be $(5.56 \pm 0.2) \times 10^5$ M^{-1} in buffered 50 mM NaCl, which is larger than $K_b = 4.7 \times 10^5$ M^{-1} reported for analogous intercalator of $[Ru(bpy)_2(Hpip)]^{2+}$ (43), 3.2-fold a K_b value of 1.7×10^5 M^{-1} for $[Ru(bpy)_2(Hbpip)]^{2+}$ (32), 11.3-fold 4.9×10^4 M^{-1} for $[Ru(bpy)_2(Haip)]^{2+}$, indicating that the introduction of pyridyl onto Hpip of the parent complex $[Ru(bpy)_2(Hpip)]^{2+}$ is very favorable for the complex to intercalate into the DNA, while the grafting of phenyl to pip was reported to be unfavorable for the DNA-binding. However, the K_b value for $[Ru(bpy)_2(Hppip)]^{2+}$ is much lower than $K_b > 10^6$ M^{-1} for $[Ru(bpy)_2(Hbopip)]^{2+}$ {Hbopip = 2-(4-benzoxazolyl)phenylimidazo[4,5-*f*][1,10] phenanthroline}(39, 70) or even dipyrido- [3,2-*a*:2',3'-*c*]phenazine (dppz)-based DNA intercalators (71, 72). The DNA binding characteristics with respect to the hypochromism, DNA binding constants, and induced red-shifts suggest that the complex in this work most likely binds to the DNA in intercalative mode, involving a strong stacking interaction between the aromatic chromophore and the base pairs of the DNA.

In addition to the electrostatic contribution, the following two factors were reported to influence DNA-binding affinity: (1) the planarity and plane area of an intercalative ligand. Good planarity of an intercalative ligand is usually advantageous for the complex binding to DNA in intercalative mode; (2) the energy (ε_{LUMO}) and population of the lowest unoccupied molecular orbital (LUMO) of the complex. As is well-established, an intercalative Ru(II) complex could act as an electron accepter, and bind to electron-donating DNA by formation of π-π stacking interactions between the intercalative ligand and DNA base pairs. Thus the lower the ε_{LUMO} of a complex is, the stronger the π-π stacking interaction between the complex and DNA would be. The related geometrical parameters of **1**, **2** (43) and **3** are shown in Table I, and the frontier molecular orbital energies of the complexes are illustrated in Scheme 3 (see Figure S1). Since the LUMO energies of the three complexes are comparable to each other, the planarity and plane area of the intercalative ligands of the complexes are expected to play a dominant role in the DNA-binding affinities. The dihedral angles in Table I show that the planarity of the main ligands of **1-3** follow the order of Hppip > Hpip >> Hbpip. The poor planarity of Hbpip is due to the steric hindrance between the hydrogen atoms on the two benzene rings of Hbpip ligand. DNA binding affinities of Hppip , Hpip and Hbpip-containing complexes of **1-3** are anticipated to follow the order of **1** > **2** >> **3**, which agrees well with the experimental observations.

Emission Spectroscopy: **1** in aerated aqueous solutions at room temperature emitted strongly with luminescence peak at ~607 nm ($\varphi = 0.046$), which is blue-shifted relative to the peaks at 628 and 632 nm reported for $[Ru(bpy)_2(Hpip)]^{2+}$ and $[Ru(bpy)_2(Hip)]^{2+}$, respectively (**43**). Changes in emission spectra of the complex with increasing DNA concentrations ([DNA] = 0-13.8 μM) was shown in Figure 3B. As the DNA was successively added into the complex solution, the emission intensities was increased moderately with an intensity enhancement factor of 0.4 ($\varphi = 0.092$) and a blue-shift in the emission peak from 607 to 603 nm at [DNA]/[Ru] ≈ 3. The DNA-binding induced emission enhancement most probably resulted from intercalative interaction since the hydrophobic environment inside the DNA helix reduced the accessibility of water molecules to the complex and the mobility of complex were restricted at the binding site, leading to a decrease in radiationless vibrational relaxation.

$[Fe(CN)_6]^{4-}$, as an excellent anionic quencher, can efficiently quenches the emissions of ruthenium complexes in the absence of the DNA due to ion pairing between the complex cations and $[Fe(CN)_6]^{4-}$ (73), but poorly quenches the emissions of

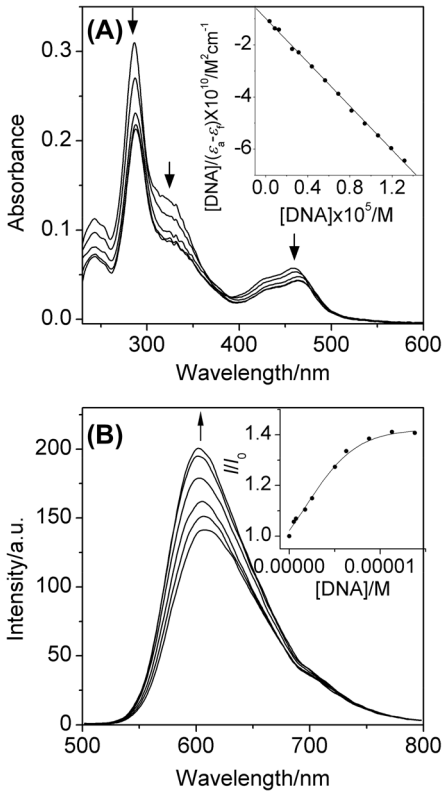

Figure 3: Changes in absorption spectra (**A**) and emission spectra (λ_{ex} = 462 nm) (**B**) of $[Ru(bpy)_2(Hppip)]^{2+}$ (5.0 μM) upon addition of ct-DNA (0-13.8 μM) in buffered 50 mM NaCl (pH = 7.10).

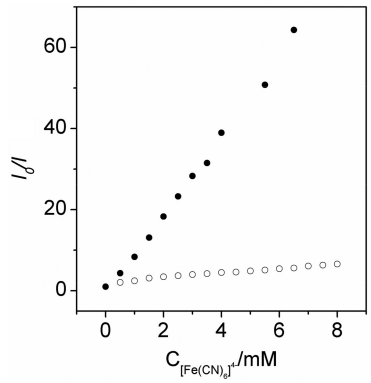

Figure 4: Emission quenching of $[Ru(bpy)_2(Hppip)]^{2+}$ (5.0 μM) with increasing concentrations of $[Fe(CN)_6]^{4-}$ (0.0-8.0 mM) in the absence of (solid squares) and the presence of (hollow squares) the DNA (20.0 μM).

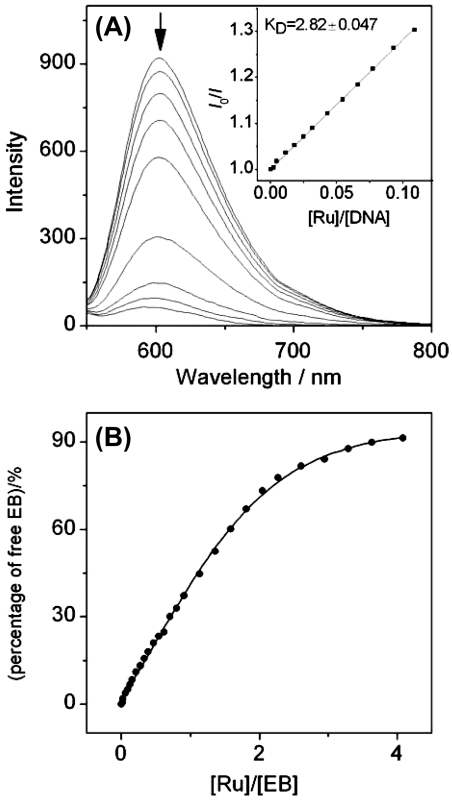

Figure 5: (**A**) Changes in emission spectra (λ_{ex} = 537 nm) of EB ([EB] = 20.0 μM) bound to DNA ([DNA] = 100.0 μM) upon successive additions of $[Ru(bpy)_2(Hppip)]^{2+}$ (0.0-90.8 μM). The arrows show the intensity changes upon increasing concentrations of the complex. Inset: florescence quenching curve of DNA-bound EB by the complex. (**B**) Plot of percentage of free EB vs. [Ru]/[EB].

ruthenium complexes intercalating into the DNA polyanion due to that the electrostatic repulsion between highly anionic $[Fe(CN)_6]^{4-}$ and DNA polyanion hinders the approaching of the quencher to the bound complex. Steady-state emission quenching experiments using $[Fe(CN)_6]^{4-}$ as the quencher can therefore be an indispensable method to study DNA binding properties of a drug molecule. Figure 4 shows Stern-Volmer plots for the emission quenching of **1** by $[Fe(CN)_6]^{4-}$ in the absence and the presence of ct-DNA. Clearly, in the absence of the DNA, the emission of **1** was efficiently quenched by $[Fe(CN)_6]^{4-}$, resulting in an almost linear Stern-Volmer plot with a slope of $(8.8 \pm 0.2) \times 10^3$ M^{-1} (K_{Q1}). However, in the presence of DNA {[DNA]/[Ru] = 4}, the slope of the quenching plot decreased remarkably to $(7.6 \pm 0.3) \times 10^2$ M^{-1} (K_{Q2}). A ratio (R) of the Stern-Volmer quenching constants, K_{Q1} to $K_{Q2,}$ is derived to be ~11.4, indicating that a better protection of **1** by the DNA probably in an intercalative mode.

The competitive binding experiments with a well-established quenching assay based on the displacement of the intercalating drug EB from ct-DNA was carried out in order to get further information regarding the DNA binding properties of 1. If **1** could be a DNA intercalator, the successive additions of **1** to the DNA pretreated with EB would cause the evident quenching in fluorescence of DNA-bound EB due to the fact that the fluorescence of the free EB (λ_{ex} = 537 nm) would be quenched by the surrounding water molecules (74). On the contrary, if the evident reduction in emission intensities of the EB-DNA system would not be observed, the complex would not be a DNA intercalator. The groove DNA binders were reported to be also capable of causing the reduction in EB emission intensities, but only moderately (75). As shown in Figure 5, additions of **1** to the EB-DNA system resulted in obvious reduction in emission intensities of EB by following the linear Sterm-Volmer equation $\{I_0/I = 1 + K_D[Ru]/[DNA]\}$ with a Stern-Volmer constant K_D of 2.82 (see inset of Figure 5A), indicating that **1** is apparently a DNA intercalator. In addition, a competitive binding model is used to calculate the apparent DNA binding constant K_{app} of 1 by using eq 4 (76)

$$K_{app} = K_{EB}([Ru]/[EB])_{50\%} \qquad [4]$$

where K_{EB} (4.94×10^5 M^{-1}) (77) is the DNA binding constant of EB, and $([Ru]/[EB])_{50\%}$ is the ratio of 1 and EB concentrations at 50% EB replacement. A K_{app} value was derived to be 8.00×10^5 M^{-1} for $[Ru(bpy)_2(Hppip)]^{2+}$, which is in agreement with the K_b value derived from UV-vis spectral titration data.

Reverse Salt Effects on DNA Binding: As anticipated from polyelectrolyte theory, the interaction of positively charged Ru(II) complex with nucleic acids would be influenced by the presence of cations or the ionic strength of the solution (78). The sensitivity to ionic strength was reported to decrease in the order of the DNA binding modes: electrostatic > groove > intercalative, which has proved a qualitative and a quantitative manner to give information on the DNA binding mode. In this study, the effects of the ionic strength on absorption and emission spectra (λ_{ex} = 462 nm) of 1 were tested by changing concentrations of NaCl in 5 mM Tirs-HCl buffer solution at pH = 7.10 (see Figure 6), and the polyelectrolyte theory was used to evaluate the relative electrostatic and nonelectrostatic contributions to the binding free energy changes. The effects of the ionic strength on the emission spectra of 1 were test by the addition of NaCl from 0 to 100 mM because the polyelectrolyte theory is strictly applicable to the system with salt concentrations lower than 0.100 M. The plot of $\log[Na^+]$ against $\log K_{obs}$ (Figure 6B) clearly shows that the binding constant values of 1 decreased with increasing salt concentrations. This is due to the stoichiometry release of sodium ion following the binding of 1 to the DNA, suggesting that electrostatic interaction is involved in the DNA-binding event. The slope of linear fitting in Figure 6(B) is equal to $-Z\psi$ in the following equation:

$$-Z\psi = \delta \log K_{obs}/\delta \log[Na^+] \quad [5]$$

where Z is the charge on the Ru(II) complex, and ψ is the fraction of counterions associated with each DNA phosphate ($\psi = 0.88$ for double-stranded B-form DNA). The Z value for the DNA-bound complex was thus derived to be 2.The Gibbs free energy change observed for DNA binding, ΔG_{obs}, can be calculated on basis of the standard Gibbs eq 6:

$$\Delta G_{obs} = -RT \ln K_{obs} \quad [6]$$

$$\Delta G_{pe} = Z\psi RT \ln[Na^+] \quad [7]$$

$$\Delta G_t = \Delta G_{obs} - \Delta G_{pe} \quad [8]$$

ΔG_{obs} can be divided into two portions, electrostatic (ΔG_{pe}) and nonelectrostatic (ΔG_t) components, which can be calculated from eqs 7 and 8, respectively. The thermodynamic binding parameters of 1 along with those reported for representative DNA binders are summarized in Table II (37, 76, 79, 80). The percent nonelectrostatic contribution to ΔG_{obs} was derived to be 53% for $[Ru(bpy)_2(Hppip)]^{2+}$ in 50 mM NaCl, which is comparable to those of the proven intercalators, such as $[Ru(bpy)_2(dppz)]^{2+}$ (79) and $[Ru(bpy)_2(Happip)]^{2+}$ (37), and much more than those of semi-intercalator $[Ru(bpy)_2(phen)]^{2+}$ (79) and electrostatically dominating $[(bpy)_2Ru(tpphz)Ru(bpy)_2]^{4+}$ (80), being consistent with the intercalative binding mode of 1.

DNA Melting Experiments: The melting of the DNA double strands into the single strand can lead to an intensity increase for the band at 260 nm, since the absorption in this wavelength for the bases of double-helical DNA is much less than that in the single form (81). And the intercalation of small molecules into the helix is known to increase the helix melting temperature (T_m), the temperature at which the double helix denatures into single-stranded DNA (82). So the DNA melting experiment offers another absolutely indispensable way to conclude how the complex binds to the DNA, intercalatively or electrostatically. The values of melting temperature, T_m, of the DNA double-strands were obtained by sigmoidal fitting of the data of percentage of single-strand DNA versus temperature. From the data shown in Figure 7, the T_m value of ct-DNA in the absence of 1 was determined to be 67.5°C and was found to increase successively upon increasing the conconcentrations of 1. However, an accurate value of DNA melting temperature change, ΔT_m, at a concentration ratio of [Ru]/[DNA] = 1:10 could not be obtained because the absorption band of DNA at 260 nm have not yet reached a platform at the maximum temperature of the instrument. A ΔT_m value of > 10°C were roughly estimated. Such a large increase in ΔT_m upon binding of 1 to the DNA, strongly supports an intercalative DNA binding mode of 1, since the classical intercalators were reported to generally give ΔT_m values of > 5°C at the concentration ratio of [DNA]/[Ru] = 10:1 (83, 84).

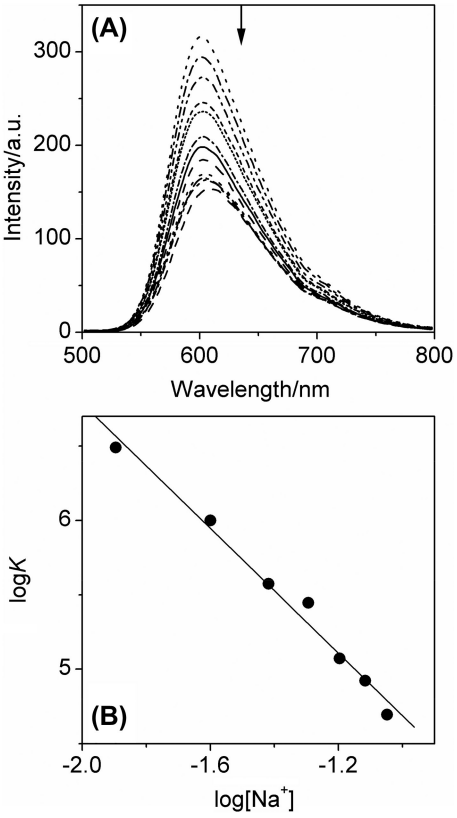

Figure 6: (**A**) Changes in emission spectra (λ_{ex} = 462 nm) of $[Ru(bpy)_2(Hppip)]^{2+}$ (5 μM) upon addition of NaCl (0-100 mM) in 5 mM Tirs-HCl buffer (pH = 7.10). (**B**) Plot of log[Na+] vs. logK_{obs} in 5 mM Tris-HCl buffer solution. The slope of this plot corresponds to the $-Z\psi$ in eq 5.

Table II
Thermodynamic DNA binding parameters[a] of K in M–1 and ΔG in kJ mol^{-1}.

DNA binder [b]	binding mode	$K_{obs}/10^3$	Z	ΔG_{obs}	ΔG_{pe}	ΔG_t ($\Delta G_t/\Delta G_{obs}$)	Ref
ethidium bromide	intercalative	494	0.85	–32.2	–5.0	–27.2 (85%)	76
$[Ru(phen)_2(dppz)]^{2+}$	intercalative	3200	2.15	–37.2	–13.8	–23.4 (63%)	79
$[Ru(bpy)_2(Happip)]^{2+}$	intercalative	295	1.51	–31.2	–9.9	–21.3 (68%)	37
$[Ru(bpy)_2(Hppip)]^{2+}$	intercalative	556	2.38	–32.8	–15.6	–17.2 (53%)	This work
$[(bpy)_2Ru(tpphz)Ru(bpy)_2]^{4+}$	electrostatic	51000	4.03	–43.5	–26.4	–17.2 (39%)	80
$[Ru(bpy)_2(phen)]^{2+}$	semi-intercalative	0.55	1.82	-15.6	-11.6	-4.0 (26%)	79

[a]In 50 mM NaCl, 5 mM Tris-HCl buffer at room temperature. [b]dppz = dipyrido[3,2-*a*:2′,3′-*c*]phenazine; phen=1,10-phenanthroline;Happip=2-(4-(β-D-allopyranoside)phenyl)imidazo[4,5-*f*][1,10]phenanthroline; tpphz = tetrapyrido-[3,2-*a*:2′,3′-*c*:3″,2″-*h*:2‴,3‴-*j*]phenazine.

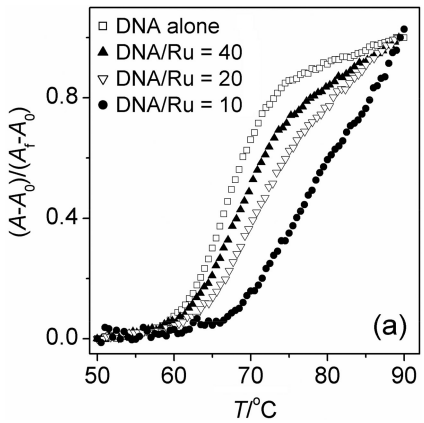

Figure 7: Thermal denaturation curves of ct-DNA (60 μM) at different concentrations of $[Ru(bpy)_2(Hppip)]^{2+}$ as shown in the left corner.

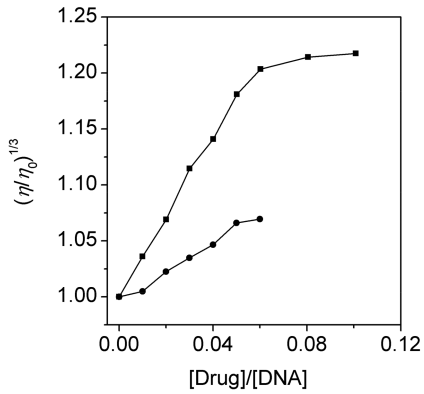

Figure 8: Effects of increasing amounts of $[Ru(bpy)_2(Hppip)]^{2+}$ (circles), and EB (squares) on the relative viscosities of ct-DNA in buffered 50 mM NaCl at 32.2°C.

DNA Viscosity Measurements: Hydrodynamic measurements, such as viscosity and sedimentation, are critical evidences for a binding mode in solution in the absence of crystallographic structural data because they are sensitive to the length changes of nucleic acids. Therefore, to probe the nature of the interaction between **1** and the DNA, the effects of the successive addition of **1** on the viscosities of aqueous ct-DNA solutions were investigated, since optical studies can not provide sufficient evidence to support the binding mode. It is well-established that a classical intercalation mode results in lengthening the DNA helix as base pairs are separated to accommodate the binding ligand, thus producing the increases in relative specific viscosity of DNA. In contrast, a partial and/or nonclassical intercalation of ligand could bend (or kink) the DNA helix, reducing its effective length and concomitantly its viscosity. In addition, electrostatic and grooving binding were reported to have little effects on DNA viscosities (17, 85). Effects of increasing amounts of **1** and EB on the relative viscosities of ct-DNA (0.2 mM) in buffered 50 mM NaCl at 32.34 ± 0.01°C are shown in Figure 8. As shown in Figure 8, the viscosities of ct-DNA increased upon successive additions of **1**, despite that the increases in the relative viscosities of the DNA are even less evident than those of the well-known DNA intercalator EB, and additions of higher concentrations of **1** were prohibited due to solubility problem, an intercalative DNA binding mode for **1** was clearly demonstrated.

Conclusions

In summery, a new Ru(II) complex of $[Ru(bpy)_2(Hppip)]^{2+}$ synthesized by grafting 2-pyridyl to $[Ru(bpy)_2(Hpip)]^{2+}$ acts as a DNA intercalator in buffered 50 mM NaCl, as evidenced by the following facts: (1) the high hypochromisms H% of 32%, 35% and 26% for absorption bands at 286, 320 and 460 nm respectively, and the large intrinsic DNA binding constant $K_b = (5.56 \pm 0.2) \times 10^5\ M^{-1}$ obtained from UV-vis spectrophotometric DNA titrations; (2) 1 was effectively protected from accessibility of the quencher $[Fe(CN)_6]^{4-}$ in the presence of DNA, as demonstrated by a large ratio of 11.4 for quenching constant derived in the absence of ct-DNA to that in the presence of the DNA; (3) the sharp decreases in emission intensities of EB-DNA system upon additions of 1, and the large apparent binding constants $K_{app} = 8.0 \times 10^5\ M^{-1}$ validated by EB competition experiment; (4) the contribution from nonelectrostatic binding (53%) to the total binding free energy; (5) the large difference of the DNA melting temperature, $\Delta T_m > 10°C$, in the absence and the presence of 1 at a concentration ratio of [DNA]/[Ru] = 10; (6) the evidently increasing trend for viscosities of ct-DNA with increasing concentrations of 1. The DFT calculations indicated that the introduction of 2-pyridyl to Hpip extends the conjugation plane of the intercalative ligand, and making 1 to bind to ct-DNA more strongly than $[Ru(bpy)_2(Hpip)]^{2+}$ (43) and $[Ru(bpy)_2(Hbpip)]^{2+}$ (32). This grafting of 2-pyridyl to Hpip also brought about pH-induced off-on-off luminescent switching of 1.

Supplementary Material

Supplementray material dealing with some frontier MOs of $[Ru(bpy)_2(Hppip)]^{2+}$ and $[Ru(bpy)_2(Hbpip)]^{2+}$ calculated by DFT-B3LYP method is available at no charge from the authors directly; the supplementary data can also be purchased from Adenine Press for US $50.00.

Acknowledgement

The authors thank the National Natural Science Foundation (Nos. 20971016, 20771016, 90922004), Beijing Natural Science Foundation (2072011), the Fundamental Research Funds for the Central Universities (2009SC-1), and Measurements Fund of Beijing Normal University for financial supports.

References

1. V. Balzani and F. Scandola. *Supramolecular Photochemistry*, Ellis Horwood, Chichester, UK, 1991.
2. G. Y. Bai, K. Z. Wang, Z. M. Duan, and L. H. Gao. *J Inorg Biochem 98*, 1017-1022 (2004).
3. V. Mahalingam, N. Chitrapriya, M. Zeller, and K. Natarajan. *Polyhedron 28*, 1532-1540 (2009).
4. D. Lawrence, V. G. Vaidyanathan, and B. U. Nair. *J Inorg Biochem 100*, 1244-1251 (2006).
5. N. A. P. Kane-Maguire and J. F. Wheeler. *Coord Chem Rev 211*, 145-162 (2001).
6. Y. Liu, R. Hammitt, D. A. Lutterman, R. P. Thummel, and C. Turro. *Inorg Chem 46*, 6011-6021 (2007).
7. P. Nagababu and S. Satyanarayana, *Polyhedron 26*, 1686-1692 (2007).
8. S. Shi, T. Xie, T. M. Yao, C. R. Wang, X. T. Geng, D. J. Yang, L. J. Han, and L. N. Ji. *Polyhedron 28*, 1355-1361 (2009).
9. A. E. Friedman, J. C. Chambron, J. P. Sauvage, N. J. Turro, and J. K. Barton. *J Am Chem Soc 112*, 4960-4962 (1990).
10. M. J. Han, Y .M. Chen, and K .Z. Wang. *New J Chem 32*, 970-980 (2008).
11. Y. M. Chen, Y. J. Liu, Q. Li, and K. Z. Wang. *J Inorg Biochem 103*, 1395-1404 (2009).
12. J. Talib, D. G. Harman, C. T. Dillon, J. Aldrich-Wright, J. L. Beck, and S. F. Ralph. *Dalton Trans*, 504-513 (2009).
13. M. J. Clarke. *Coord Chem Rev 236*, 209-233 (2003).
14. V. Rajendiran, M. Murali, E. Suresh, S. Sinha, K. Somasundaramc, and M. Palaniandavar. *Dalton Trans* 148-163 (2008).
15. V. Rajendiran, M. Murali, E. Suresh, M. Palaniandavar, V. S. Periasamyc, and M. A. Akbarshac. *Dalton Trans*, 2157-2170 (2008).
16. H. Xu, K. C. Zheng, Y Chen, Y. Z. Li, L. J. Lin, H. Li, P. X. Zhang, and L. N. Ji. *Dalton Trans* 2260-2268 (2003).
17. P. U. Maheswari, V. Rajendiran, M. Palaniandavar, R. Parthasarathi, and V. Subramanian. *J Inorg Biochem 100*, 3-17 (2006).
18. K. Bhadra and G. S. Kumar. *Mini Rev Med Chem 10,* 1235-1247 (2010).
19. M. Maiti and G. S. Kumar. *Med Res Rev 27*, 649-695 (2007).
20. J. G. Liu, Q. L. Zhang, X. F. Shi, and L. N. Ji. *Inorg Chem 40*, 5045-5050 (2001).
21. C. S. Chow and J. K. Barton. *J Am Chem Soc 112*, 2839-2841 (1990).
22. X. Qu and J. B. Chaires. *J Am Chem Soc 123*, 1-7 (2001).
23. B. Saha, A. Mukherjee, C. R. Santra, A. Chattopadhyay, A. N. Ghosh, U. Choudhuri, and P. Karmakar. *J Biomol Struct Dyn 26*, 421-429 (2009).
24. G. Singhal and M. R. Rajeswari. *J Biomol Struct Dyn 26*, 625-636 (2009).
25. Y. Dalyan, I. Vardanyan, A. Chavushyan, and G. Balayan. *J Biomol Struct Dyn 28*, 123-131 (2010).
26. N. P. Bazhulina, A. M. Nikitin, S. A. Rodin, A. N. Surovaya, Yu. V. Kravatsky, V. F. Pismensky, V. S. Archipova, R. Martin, and G. V. Gursky. *J Biomol Struct Dyn 26*, 701-718 (2009).
27. P. Sharma, S. Sharma, A. Mitra, and H. Singh. *J Biomol Struct Dyn 27*, 65-81 (2009).
28. D. Vasilescu, M. Adrian–Scotto, A. Fadiel, and A. Hamza. *J Biomol Struct Dyn 27*, 465-476 (2010).
29. B. Jin, H. M. Lee, and S. K. Kim. *J Biomol Struct Dyn 27*, 457-464 (2010).
30. H. M. Lee, B. Jin, S. W. Han, and S. K. Kim. *J Biomol Struct Dyn 28*, 421-430 (2010).
31. L. C. Xu, J. Li, S. Shi, K. C Zheng, and L. N. Ji. *J Mol Struct (THEOCHEM) 855*, 77-81 (2008).
32. L. F. Tan, H. Chao, Y. F. Zhou, and L. N. Ji. *Polyhedron 26*, 3029-3036 (2007).
33. L. C. Xu, S. Shi, J. Li, S. Y. Liao, K. C. Zheng, and L. N. Ji. *Dalton Trans* 291-301 (2008).
34. B. Sun, J. X. Guan, L. Xu, B. L. Yu, L. Jiang, J. F. Kou, L. Wang, X. D. Ding, H. Chao, and L. N. Ji. *Inorg Chem 48,* 4637-4639 (2009).
35. M. J. Han, L. H. Gao, and K. Z. Wang. *New J Chem 30*, 208-214 (2006).
36. Y. Y. Lü , L. H. Gao, M. J. Han, and K. Z. Wang. *Eur J Inorg Chem* 430-436 (2006).
37. Y. Z. Ma, H. J. Yin, and K. Z. Wang. *J Phys Chem B 113*, 11039-11047 (2009).
38. M. J. Han, L. H. Gao, Y. Y. Lü, and K. Z. Wang. *J Phys Chem B 110*, 2364-2371 (2006).
39. F. R. Liu, K. Z. Wang, G. Y. Bai, Y. A. Zhang, and L. H. Gao. *Inorg Chem 43*, 1799-1806 (2004).
40. M. J. Han, Z. M. Duan, Q. Hao, S. Z. Zheng, and K. Z. Wang. *J Phys Chem C 111*, 16577-16585 (2007).
41. B. Y. Wu, L. H. Gao, Z. M. Duan, and K. Z. Wang. *J Inorg Biochem 99*, 1685-1691 (2005).
42. G. Y. Bai, K. Z. Wang, Z. M. Duan, and L. H. Gao. *J Inorg Biochem 98*, 1017-1022 (2004).
43. K. C. Zheng, H. Deng, X. W. Liu, H. Li, H. Chao, and L. N. Ji. *J Mol Struct (Theochem) 682*, 225-233 (2004).

44. J. B. Foresman and M. J. Frisch, *Exploring Chemistry with Electronic Structure Methods*, 2nd ed.; Gaussian Inc.: Pittsburgh, PA, 1996.
45. N. Kurita and K. Kobayashi. *Comput Chem 24*, 351-357 (2000).
46. G. Pourtois, D. Beljonne, C. Moucheron, S. Schumm, A. Kirsch De Mesmaeker, R. Lazzaroni, and J. L. Bredas. *J Am Chem Soc 126*, 683-692 (2004).
47. M. K. Nazeeruddin, F. De Angelis, S. Fantacci, A. Selloni, G. Viscardi, P. Liska, S. Ito, B. Takeru, and M. Gratzel. *J Am Chem Soc 127*, 16835-16847 (2005).
48. M. N. Ackermann and L. V. Interrante. *Inorg Chem 23*, 3904-3911 (1984).
49. A. M. Pyle, M. Y. Chiang, and J. K. Barton. *Inorg Chem 29*, 4487-4495 (1990).
50. D. D. Perrin, W. L. Armarego, and D. R. Perrin. *Purification of Laboratory Chemicals*, 2nd ed., Pergamon, Oxford, 1980.
51. J. V. Houten and R. J. Watts. *J Am Chem Soc 98*, 4853-4858 (1976).
52. M. E. Reichmann, C. A. Rice, C. A. Thomas, and P. Doty. *J Am Chem Soc 76*, 3047-3053 (1954).
53. J. B. Chaires, N. Dattagupta, and D. M. Crothers. *Biochemistry 21*, 3933-3940 (1982).
54. X. H. Zou, B. H. Ye, H. Li, J. G. Liu, Y. Xiong, and L. N. Ji. *J Chem Soc Dalton Trans* 1423-1428 (1999).
55. A. Gorling. *Phys Rev 54*, 3912-3915 (1996).
56. P. J. Hay and W. R. Wadt. *J Chem Phys 82*, 270-283 (1985).
57. A. Juris, V. Balzani, F. Barigelletti, S. Campagna, P. Belser, and A. V. Zelewsky. *Coord Chem Rev 84*, 85-277 (1988).
58. M. J. Frisch. Gaussian 03 Revision D.01, Gaussian Inc, Wallingford CT, 2005.
59. A. M. W. C. Thompson, M. C. C. Smailes, J. C. Jeffery, and M. D. Ward. *J Chem Soc Dalton Trans* 737-743 (1997).
60. H. Cao, B. H. Ye, H. Li, R. H. Li, J. Y. Zhou, and L. N. Ji. *Polyhedron 19*, 1975-1983 (2000).
61. R. Grigg and W. D. J. A. Norbert. *J Chem Soc Chem Commun* 1300-1302 (1992).
62. E. C. Constable, M. J. Hannon, A. M. W. Cargill Thompson, D. A. Tocher, and J. V. Walker. Supramol Chem 2, 243-246 (1993).
63. R. H. Fabian, D. M. Klassen, and R. W. Sonntag. *Inorg Chem 19*, 1977-1982 (1980).
64. J. M. Kelly, C. Long, C. M. O'Connell, J. M. Vos, and H. A. Tinnemans. *Inorg Chem 22*, 2818-2824 (1983).
65. J. G. Vos. *Polyhedron 11*, 2285-2299 (1992).
66. J. Z. Wu, L. Li, T. X. Zeng, L. N. Ji, J. Y. Zhou, T. Luo, and R. H. Li. *Polyhedron 16*, 103-107 (1997).
67. J. Z. Wu, B. H. Ye, L. Wang, L. N. Ji, J. Y. Zhou, R. H. Li, and Z. Y. Zhou. *J Chem Soc Dalton Trans* 1395-1401 (1997).
68. S. Shi, J. Liu, J. Li, K. C. Zheng, C. P. Tan, L. M. Chen, and L. N. Ji. *Dalton Trans* 2038-2046 (2005).
69. A. Wolf, G. H. Jr. Shimer, and T. Meehan. *Biochemistry 26*, 6392-6396 (1987).
70. Q. Hao, Z. M. Duan, M. J. Han, S. Z. Zheng, Y. Y. Lu, and K. Z. Wang. *Gaodeng Xuexiao Huaxue Xuebao (in Chinese) 27*, 1217-1219 (2006).
71. D. L. Carlson, D. H. Huchital, E. J. Mantilla, R. D. Sheardy, and W. R. Murphy. *J Am Chem Soc 115*, 6424-6425 (1993).
72. P. Lincoln, A. Broo, and B. Norden. *J Am Chem Soc 118*, 2644-2653 (1996).
73. J. K. Barton, J. M. Goldberg, C. V. Kumar, and N. J. Turro. *J Am Chem Soc 108*, 2081-2088 (1986).
74. I. Ortmans, B. Elias, J. M. Kelly, C. Moucheron, and A. Kirsch-DeMesmaeker. *Dalton Trans 4*, 668-676 (2004).
75. J. M. Kelly, A. B. Tossi, D. J. Meconnell, and C. Ohuigin. *Nucleic Acids Res 13*, 6017-6034 (1985).
76. D. L. Boger, B. E. Fink, S. R. Brunette, W. C. Tse, and M. P. Hedrick. *J Am Chem Soc 123*, 5878-5891 (2001).
77. M. K. Wijaya, E. T. Wahyuni, N. Yoshioka, and H. Inoue. *Biophys Chem 121*, 44-50 (2006).
78. M. T. Record, T. M. Lohman, and P. De Haseth. *J Mol Biol 107*, 145-158 (1976).
79. F. Pierard, A. Del Guerzo, A. Kirsch-De Mesmaeker, M. Demeunynck, and J. Lhomme. *Phys Chem Chem Phys 3*, 2911-2920 (2001).
80. D. A. Lutterman, A. Chouai, Y. Liu, Y. J. Sun, C. D. Stewart, K. R. Dunbar, and C. Turro. *J Am Chem Soc 130*, 1163-1170 (2008).
81. C. V. Kumar and E. H. Asuncion. *J Am Chem Soc 115*, 8547-8553 (1993).
82. D. J. Patel. *Acc Chem Res 12*, 118-125 (1979).
83. S. J. Heater, M. W. Carrano, D. Rains, R. B. Walter, D. Ji, Q. Yan, R. S. Czernuszewic, and C. Carrano. *Inorg Chem 39*, 3881-3889 (2000).
84. C. M. Dupureur and J. K. Barton. *Inorg Chem 36*, 33-43 (1997).
85. L. Lerman. *J Mol Biol 3*, 18-30 (1961).

Date Received: October 6, 2010

Communicated by the Editor Ramaswamy H. Sarma